Simulation of Rotating Stall by the Vortex Method

Philippe R. Spalart*
NASA Ames Research Center, Moffett Field, California

The vortex method, coupled to a boundary-layer solver, is applied to the numerical simulation of high Reynolds number incompressible flow in two-dimensional cascades. Periodic conditions are imposed along the plane of the cascade, with several blades per period. Good agreement is found with two finite-difference methods for a single-blade case. When a staggered cascade is treated with five independent blades, the simulation predicts rotating stall, for a range of angles of attack and stagger, and the essential features of the flow are correct. The stall cell steadily propagates along the cascade. The sensitivity of this phenomenon to two parameters is studied, and the stall boundary is found. Quantitative results and visualizations are presented.

I. Introduction

THE vortex method and computers have been improved enough so that one can treat practical cases, for engineering applications, in two dimensions. Runs taking on the order of 15 min on a Cray allow a useful simulation of the time-dependent flow around a bluff body or stalled airfoil at high Reynolds numbers. Examples of flows of aeronautical interest that have been treated include the dynamic stall of airfoils,[1] airfoils with spoilers, and airfoils at large angles of attack.[2]

The "vortex blob" method[3] is well established and robust. It requires relatively little computer memory. When the boundary conditions are treated using an integral equation, instead of image vortices, complex geometries and multibodies can be treated.[1] Coupling the vortex method with a boundary-layer solver allows it to capture the major effects of transition and separation.[1] In many cases equivalent simulations are not practical with other methods, such as finite-difference methods. Generating grids becomes very difficult when complex shapes are involved. The difficulty in solving the equations also increases with the Reynolds number.

On the other hand, experience shows that while the vortex method can provide useful results for all these flows, an overall accuracy of, say, 10% is still far from being consistently achieved.[2] This must be improved before the method is accepted and widely used. The vortex method is very stable and can be used, formally, at very high Reynolds numbers, but with a few thousand vortices it clearly cannot describe all the scales of a turbulent flow. Another weakness of the vortex method is the difficulty in extending it to three-dimensional or compressible flows.

The method used for this study was first described in Ref. 1 and used in Refs. 2 and 4. It has been tested over a wide range of shapes, with varying degrees of success. The shedding frequency is generally better predicted than the drag. The method gave good results for the forces on an oscillating airfoil.[1,4] Encouraging results were also obtained for the circular cylinder by coupling the vortex method with a finite-difference boundary-layer solver.[4] The method is less successful when treating other shapes.[2] It overpredicts the drag of an equilateral triangle but underpredicts the drag of a square, even when the two calculations are conducted with exactly the same set of parameters. Thus a one-sided correction like a circulation reduction, besides violating the equations, would not improve the overall performance of the method (this issue is somewhat controversial).

There is no strong evidence that the three-dimensional effects present in the experiments are responsible for the discrepancies. The sensitivity of the results to numerical parameters like the time step, number of vortices, and core radius and profile has been found to be very weak over large ranges of variation. In the long run, submitting the method to specific tests until a pattern is found will be more useful than introducing "fudge factors" and will turn the vortex method into a truly predictive method.

This paper describes the treatment of cascades by a periodic version of the vortex method. The best application so far is the simulation of rotating stall. The problem of rotating stall is very important for the performance and reliability of jet engines; it was already present in 1944 on the Me 262. When the load on the compressor is high or suddenly increases, stall can occur, and sometimes the engine has to be totally shut down and restarted. Rotating stall involves complex interactions between the blades of a staggered cascade and is an essentially unsolved problem.

For the rotating stall simulations, several blades are included in the computational domain and the vortex method fully utilizes its ability to simulate the flow in complex, multiply connected domains. It is well known that, even with a geometry that is perfectly periodic from blade to blade, the solution that has this periodicity may be unstable to disturbances having a longer period. Such an instability actually occurs for certain geometries and is the origin of the rotating stall phenomenon. This study seems to be the first example of rotating stall obtained as the result of systematic numerical simulations. The instability can be triggered either by a weak explicit initial disturbance (a dipole) or by numerical disturbances. As the simulation advances in time, a strongly nonlinear, large-amplitude disturbance develops and then essentially preserves itself while traveling along the cascade.

In the simulations the physical situation is considerably simplified compared with the situation in an engine compressor. The effects of compressibility, three-dimensionality, rotation, and upstream disturbances are ignored. The objective is mostly to gain physical insight; quantitative information should not be expected, at least at this stage (two-dimensional experiments are also unavailable, for obvious reasons). It is valuable to know that rotating stall can be described by as simple a model as the two-dimensional, incompressible Navier-Stokes equations.

Received Jan. 23, 1984; revision received Sept. 19, 1984.

*National Research Council Research Associate, Computational Fluid Dynamics Branch.

II. Numerical Method

The method used for this study is very similar to the one described in Ref. 1. Converting a vortex code from treating isolated bodies to treating periodic cascades is straightforward. Each element now represents a periodic array of vortices instead of a single vortex. The stream function induced by such an array is given by Lamb.[5] If the vortex is at a complex position z_0 and has circulation Γ, the stream function at z, instead of $\Gamma/2\pi\log(|z-z_0|)$, is

$$\Psi(z)=\frac{\Gamma}{2\pi}\log\left[\left|\sin\left(\frac{2\pi i(z-z_0)}{p}\right)\right|\right] \tag{1}$$

This new function is periodic with period p in the y direction and has the same singularity at z_0. Clearly the short-range interactions are not affected, since for small $(z-z_0)$ the difference between $\sin(z-z_0)$ and $(z-z_0)$ is of third order. The long-range interactions, on the other hand, are very different. The induced velocity does not tend to 0 at infinity in the x direction, but to constant values $\pm\Gamma/2p$. In addition, the velocity tends to these values exponentially fast, whereas the decay was algebraic in the single-vortex case. This means that the flow induced by a dipole, for instance, decays exponentially in the x direction.

The evaluation of the interactions, by application of the Biot-Savart law, now requires the computation of complex exponentials, which could be very expensive. However, these exponentials can be precomputed, at a cost of order N_v, and the $O(N_v^2)$ part (the bulk of the work, with a vortex method) is then reduced to complex multiplications. N_v is the number of vortices. As a result, the periodic code is not much slower than the nonperiodic code, for the same number of vortices. The CPU time is 1.6 s/time step, with 1600 vortices, on a Cray X-MP computer.

The smoothing of the velocity field by a core or blob is done in a way very similar to the nonperiodic code. The singular stream function defined by Eq. (1) is replaced by

$$\Psi_\sigma(z)=\frac{\Gamma}{4\pi}\log\left[\left|\sin\left(\frac{2\pi i(z-z_0)}{p}\right)\right|^2+\sigma^2\right] \tag{2}$$

which has the same behavior away from z_0, and is regular at z_0. σ is the core radius. This type of core is the simplest to use and the fastest to compute.[4]

The merging vortices is also done by directly adapting the device from the nonperiodic code.[1] Merging vortices is necessary because of numerical considerations: the need to compensate the creation of new vortices at the wall at every time step. The device is based on a Taylor expansion of the disturbance caused by the merging.[4]

The boundary layer is treated by simple integral methods up to the point of separation, with a quasi-steady approximation, as in Ref. 1. A finer determination of the stall boundary would probably require a more elaborate boundary-layer model, as well as some information about the upstream turbulence, wall roughness, etc. The vortices created along the attached part of the boundary layer will not be released into the flow. The boundary-layer calculation is stopped upstream of the separation point in order to avoid the associated singularity. The separation region and the wake are handled by the vortices. This is not affected by the periodicity assumption. However, locating the attachment point is more delicate than for isolated bodies. With an isolated body there is almost always a well-defined attachment point near the leading edge, with irrotational flow in its vicinity. With stalled flow in a cascade, the flow next to a blade, even upstream of it, can be greatly disturbed by the neighboring blades (see Fig. 6b). As a result, the attachment point behaves erratically, or several attachment points exist, etc. If at a given time step the apparent attachment point found by the program (by seeking the highest pressure) does not fall reasonably close to the leading edge, the

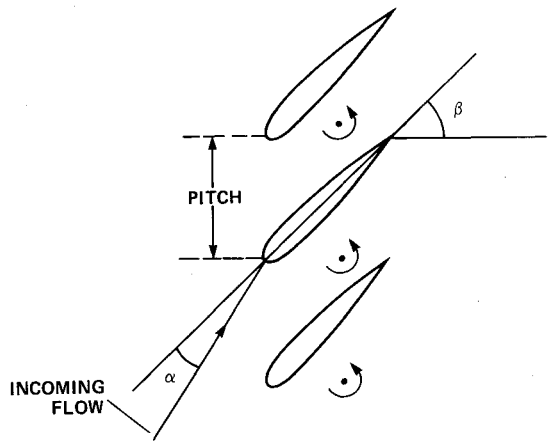

Fig. 1 Geometry of cascade.

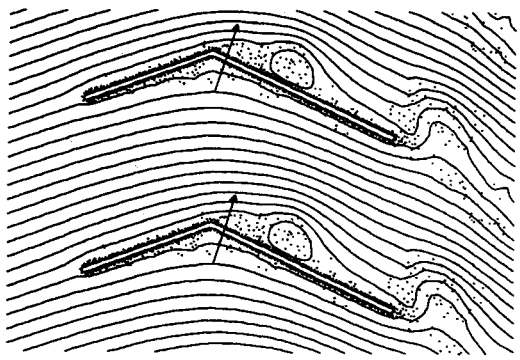

Fig. 2 Instantaneous flow pattern in cascade.

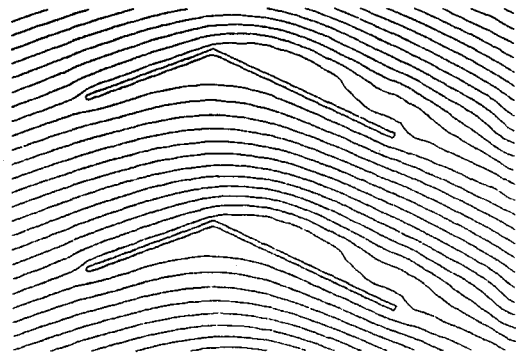

Fig. 3 Average flow pattern in cascade.

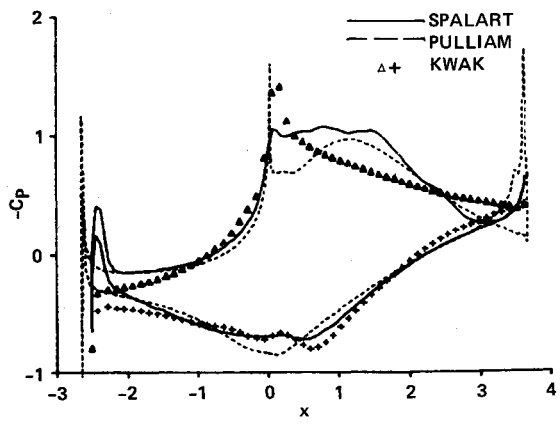

Fig. 4 Average pressure distribution on cascade.

flow is assumed to be fully separated for that blade. The boundary-layer calculation is then bypassed, and all the new vortices emitted by that blade for this step are released into the flow.

There are a few other differences between the code used here and the one described in Ref. 1, unrelated to the periodic conditions. The pressure is computed more accurately. The vortex core function, defined by Eq. (2), is simpler.[4] Taylor expansions are not used any more in the computation of the interactions, because the resulting short loops were not efficient on a vector computer like the Cray (the computations reported in Ref. 1 were done on a CDC 7600). With the straightforward $O(N_v^2)$ Biot-Savart algorithm, vortex codes vectorize very well. The time-consuming loops are long, 1000 or more.

The value of the main parameters, nondimensionalized by the chord and inflow velocity, are: time step $\Delta t = 0.02$, $\sigma = 0.006$, number of wall points $N_\omega = 100$ per blade, and $N_v = 300$ per blade.

The physical assumptions are the following. The blade shape and stagger angle, and the pitch, are input. They are defined in Fig. 1. The number of blades per period is assumed: it should be large enough to allow stall cells to develop, but it is limited by cost considerations. Five blades proved sufficient; running the code with more blades should be considered when more specific questions can be asked. The main question is: What is the most natural period for the phenomenon? Including more than about 10 blades would be quite impractical.

The inflow angle is a normal input to a cascade simulation. The outflow angle and pressure, lift and drag coefficients, and loss of total pressure are results of the simulation. The initial condition is potential flow with zero circulation around each blade. A weak dipole is sometimes added in the wake as a disturbance to trigger the instability that leads to rotating stall.

The cascade code was tested on a cascade made of two thin plates, hinged at about 40% of the chord. These turning vanes were used in the NASA Ames Research Center $40 \times 80 \times 120$ wind tunnel and were the cause of an accident. The simulation predicted unsteady flow with shedding of vortices from the upper surface at the hinge and a separation bubble under the hinge, as shown in Fig. 2. Figure 2 displays the blade, the vortices, the streamlines, and the force vector at a given time. The figure shows two identical periods. The steamlines of the time-averaged velocity field are shown in Fig. 3. There is reattachment in the average on the upper and lower surfaces, which is an effect of the Reynolds shear stresses. The average pressure distribution was compared with unpublished finite-difference results by Pulliam and Kwak (NASA Ames Research Center, personal communication). Pulliam used a compressible method at low Mach number and a turbulence model, while Kwak used an incompressible method and treated the flow as laminar at a lower Reynolds number. Their results were of a preliminary nature. Figure 4 presents a comparison of the average pressure distributions: the agreement between the three methods is good.

III. Rotating Stall Simulations

The configuration for the rotating stall simulations was suggested by Dr. J. Adamczyk (NASA Lewis Research Center). Thin noncambered airfoils were used, with a pitch equal to 1 chord length. All the simulations but one used five blades per period. Two parameters—the stagger angle β and the angle of attack α were varied (see Fig. 1). Typical cascade airfoils are

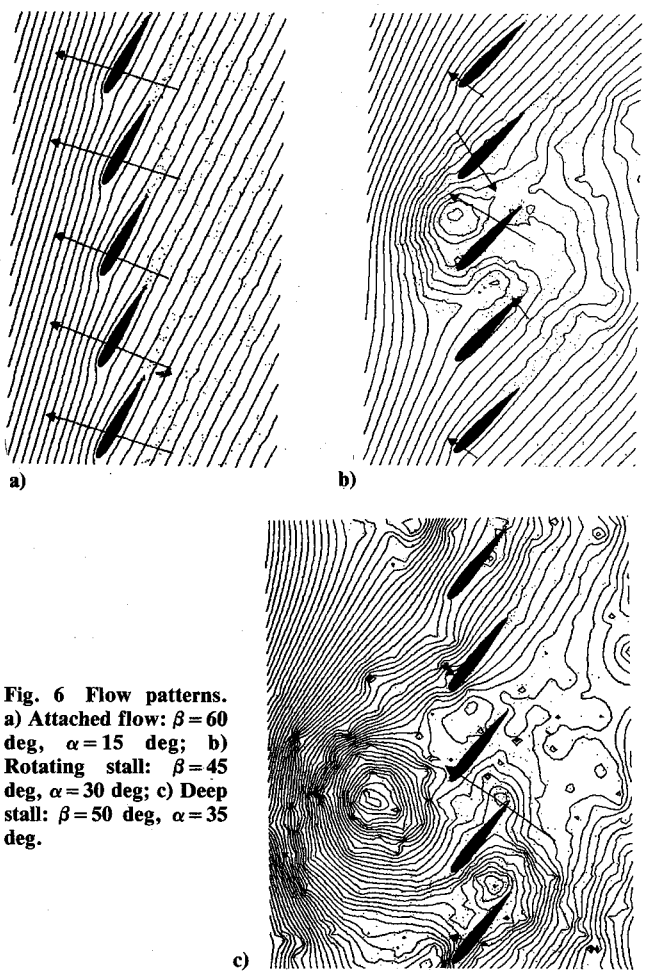

Fig. 6 Flow patterns. a) Attached flow: $\beta = 60$ deg, $\alpha = 15$ deg; b) Rotating stall: $\beta = 45$ deg, $\alpha = 30$ deg; c) Deep stall: $\beta = 50$ deg, $\alpha = 35$ deg.

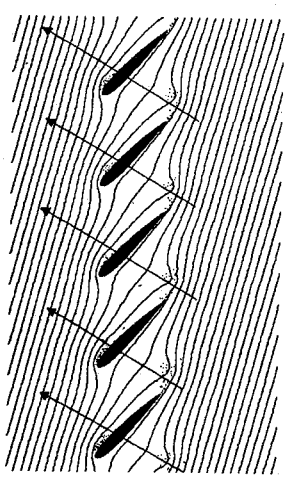

Fig. 5 Flow pattern shortly after impulsive start, $\beta = 45$ deg, $\alpha = 30$ deg.

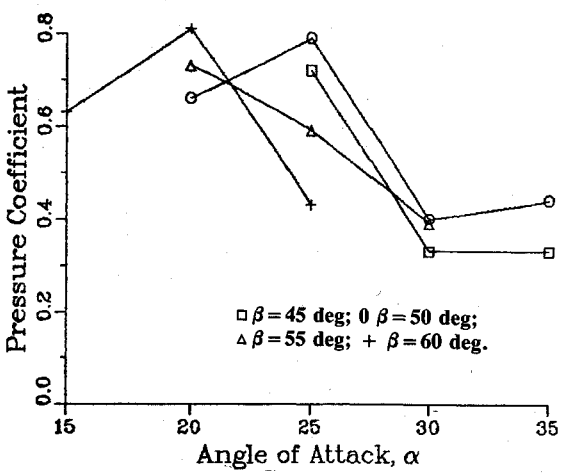

Fig. 7 Pressure rise.

rather thin but have some camber; however, camber was not included in this study to reduce the number of parameters. The pitch equal to 1 chord was chosen to give a fairly low solidity, which is known to promote stall. The two parameters α and β were chosen because they were expected to have the strongest effect on the stall. The angle β was rather high, between 45 and 65 deg, so that the cascade was strongly staggered. The angle of attack α was between 15 and 35 deg.

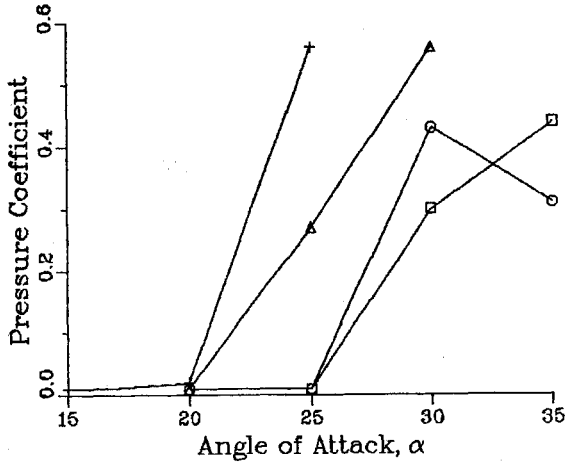

Fig. 8 Loss of total pressure, $\beta = 45$ deg, $\beta = 50$ deg, $\beta = 55$ deg, $\beta = 60$ deg.

Some preliminary simulations were made with flat plates or thinner NACA airfoils, but all the runs reported here were with the NACA 0012 airfoil. The results with flat plates were similar, but fully attached flow was not possible on the upper surface. As a result, the loss of total pressure was higher.

The simulations produce qualitative and quantitative results. Plots of the vortices and streamlines clearly show the stall pattern, its inception, and its propagation. This propagation is also reflected by the time-dependent forces. The quantitative results also include the time-average pressure rise across the cascade and the loss of total pressure. This loss is 0 in an attached flow and is a good measure of the efficiency of the cascade.

Figure 5 shows the flow shortly after the beginning of the simulation. Each blade is seen to release a starting vortex. This figure also shows that the initial disturbance is very weak. The early part of the simulation is a transient regime during which a starting vortex is formed, the circulation around the blades is established, and the nonuniform character of the flow possibly develops. Most of the results that will be shown were taken after this transient, which takes on the order of 10 time units at least (nondimensionalized by velocity and chord). If the dipole is omitted (and if the geometry is right), the instability is still observed but takes more time.

Figure 6 displays the different flow patterns that emerged from the study. In Fig. 6a, with $\beta = 60$ deg and $\alpha = 15$ deg, the flow is fully attached on each blade and is the same from blade to blade. In Fig. 6b, with $\beta = 45$ deg and $\alpha = 30$ deg, the flow is very different from one blade to the next. The flow near some blades is attached, while it is clearly stalled over the other blades. There is a "stall cell." More details will be given later.

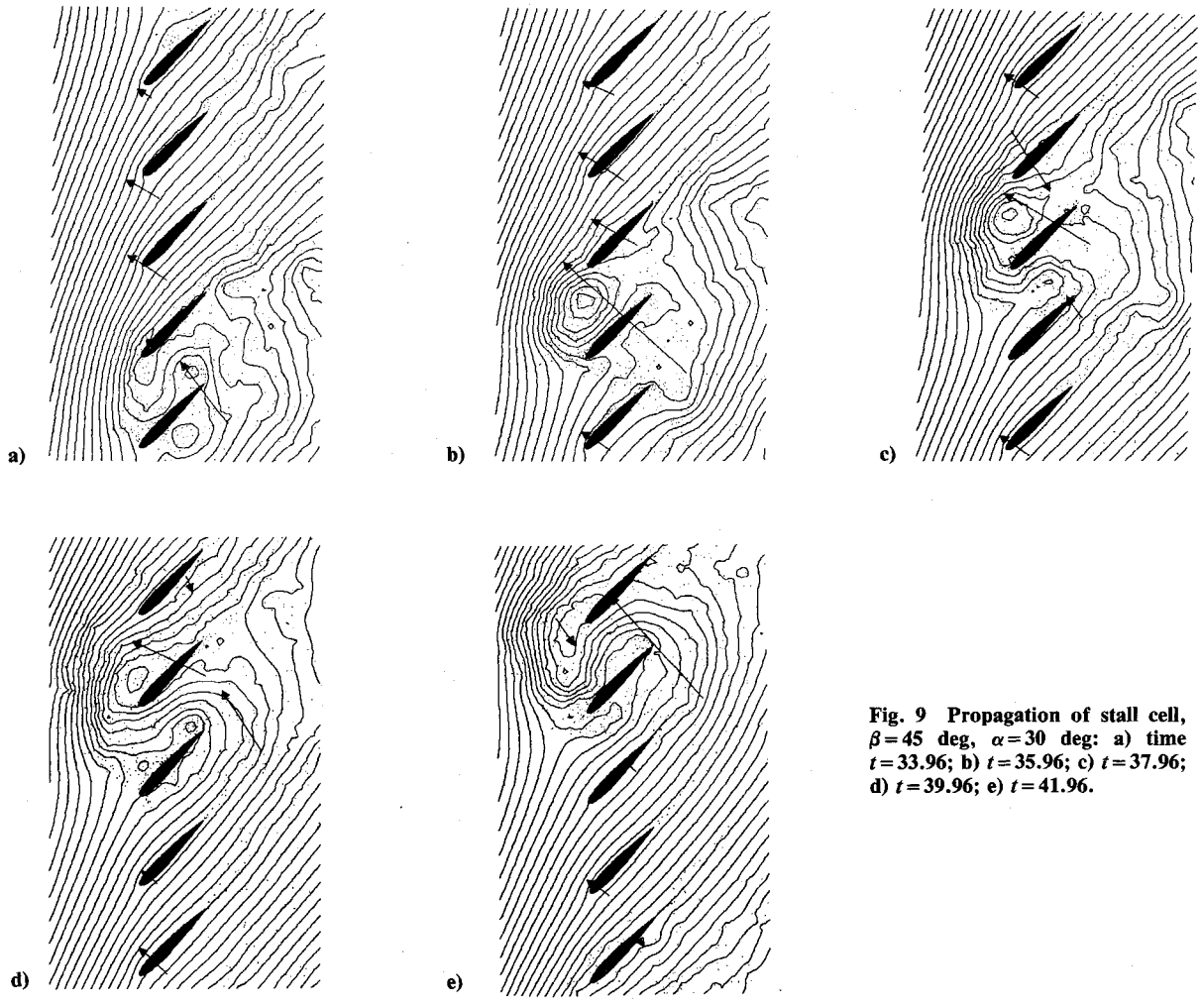

Fig. 9 Propagation of stall cell, $\beta = 45$ deg, $\alpha = 30$ deg: a) time $t = 33.96$; b) $t = 35.96$; c) $t = 37.96$; d) $t = 39.96$; e) $t = 41.96$.

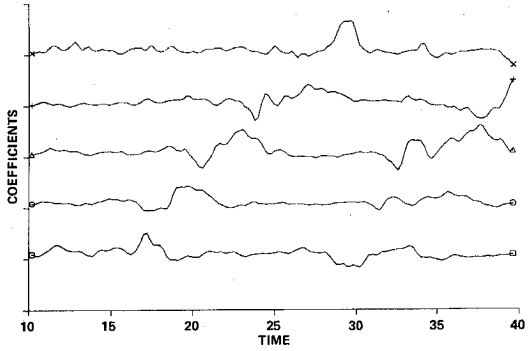

Fig. 10 Normal force on the five blades, $\beta = 45$ deg, $\alpha = 30$ deg: □ blade 1; 0 blade 2; Δ blade 3; + blade 4; × blade 5.

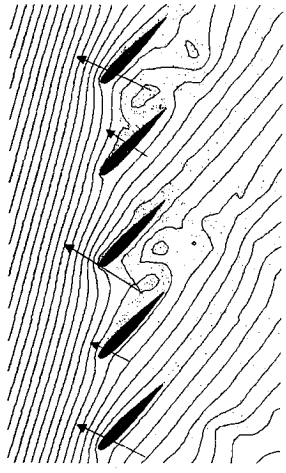

Fig. 11 Two stall cells, $\beta = 55$ deg, $\alpha = 25$ deg.

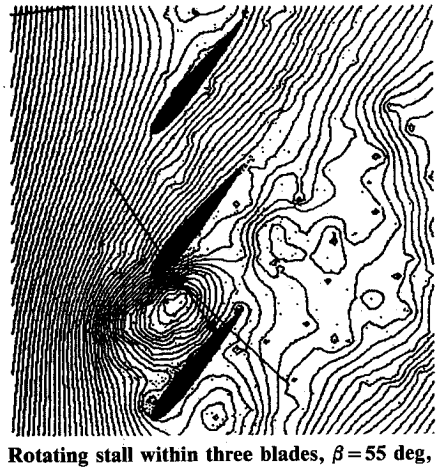

Fig. 12 Rotating stall within three blades, $\beta = 55$ deg, $\alpha = 25$ deg.

Figure 6c shows the deep stall situation, $\beta = 50$ deg and $\alpha = 35$ deg. A large clockwise vortex forms and propagates, but now in front of the cascade. It does not go through the cascade as in the previous case, and seems to grow continuously larger. This occurs at very high values of α and β (inflow angle 85 deg), which might not be very realistic.

Table 1 shows the 13 cases that were run; the flow pattern is indicated by a letter. A means attached flow or light separation over the trailing edge, as in Fig. 6a; R means rotating stall, as in Fig. 6b; and D means deep stall, as in Fig. 6c. Three regions appear in Table 1, and the flow is more and more stalled as α and β increase, as was expected. The boundary between A and R is very clear, more so than the boundary between R and D. The stall boundary follows approximately the $\alpha + \beta/3 = 42.5$ deg line. Thus, stagger seems to promote rotating stall for a given airfoil, solidity, and angle of attack.

Table 1

β	45	50	55	60
α				
35	D	D		
30	R	R	D	
25	A	A	R	D
20		A	A	A
15				A

The time-average quantities are plotted in Figs. 7 and 8. Figure 7 shows the pressure rise as a function of α for each value of β, and Fig. 8 shows the corresponding loss of total pressure. Both quantities are nondimensional, based on the incoming dynamic pressure. Flows of type A have pressure rises of the order of 0.6 to 0.8 and loss coefficients of about 0.01. Flows of type R and D have pressure rises of about 0.3 to 0.6 and loss coefficients of the order of 0.3 to 0.6. The loss coefficient is a sensitive indicator of stall.

The R pattern is the one of most interest, since it is close to the boundary with attached flow, and will now be described in more detail. Figure 9 shows the state of the flow at different times; $\beta = 45$ deg and $\alpha = 30$ deg. The nondimensional time elapsed between each picture is 2, based on the chord and the magnitude of the incoming velocity. The stall cell is seen to move upward, and the propagation velocity is about 0.4 times the incoming velocity. With $\beta = 50$ deg, $\alpha = 30$ deg this velocity is about 0.5.

The streamlines reveal large vortices of opposite sense in the flow. By counting the streamlines it can also be seen that the mass flux is high between the attached blades and low, or even negative, between the stalled blades. The flow chokes in this passage, and the fluid is forced to escape through the other passages. The mechanism responsible for the propagation probably works in the following manner: as a blade stalls, it releases a large clockwise vortex which displaces the flow and increases the angle of attack of the next blade up. This causes this blade to stall. Furthermore, the constriction of this passage also deflects fluid down and reduces the angle of attack of the next blade down, thus helping this blade reattach. The counterclockwise vortex is released from the trailing edge and has less influence.

The flow pattern compares favorably with a movie made by Stenning at M.I.T. in 1956 (J. Adamczyk, personal communication). The experiment was in a circular compressor, with cambered airfoils, and the flow was at least slightly compressible, since interferometer and schlieren techniques were used. The movie shows a periodic evolution, and the distance between stall cells is about 4 to 6 blades. The visualization clearly shows vortices of opposite sense being released from the leading and trailing edges. It would be hard to estimate the propagation velocity from the movie.

Figure 10 shows the time-dependent normal force on the five blades. The propagation of the stall cell is reflected by a surge in the force on the individual blades. This surge reappears at the bottom of the period after leaving through the top. The signal in Fig. 10 has been filtered to suppress high-frequency noise.

There were a few examples in which a different rotating stall pattern was observed ($\beta = 55$ deg, $\alpha = 25$ deg or $\beta = 50$ deg, $\alpha = 30$ deg). The flow developed two stall cells instead of one, as shown in Fig. 11. However, when the simulation was continued long enough, the pattern eventually changed to a one-cell pattern. This transition was slow, taking on the order of 10 to 20 time units. This indicates that the one-cell pattern is more stable than the two-cell pattern, but it also suggests that rotating stall is possible within less than five blades. To confirm this, the same case was run again with only three blades. As can be seen in Fig. 12, rotating stall still occurred.

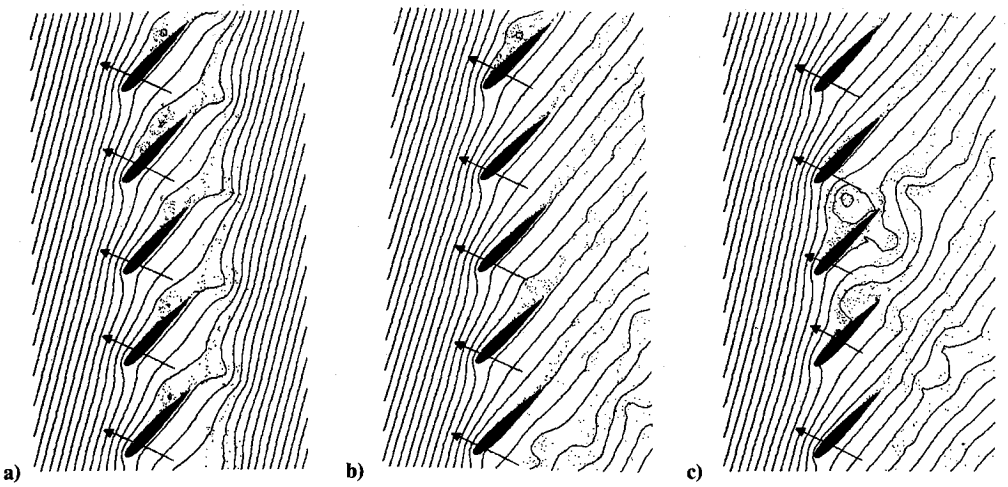

Fig. 13 Simulation started without initial disturbance: a) $t=1.98$, b) $t=7.98$, c) $t=21.96$.

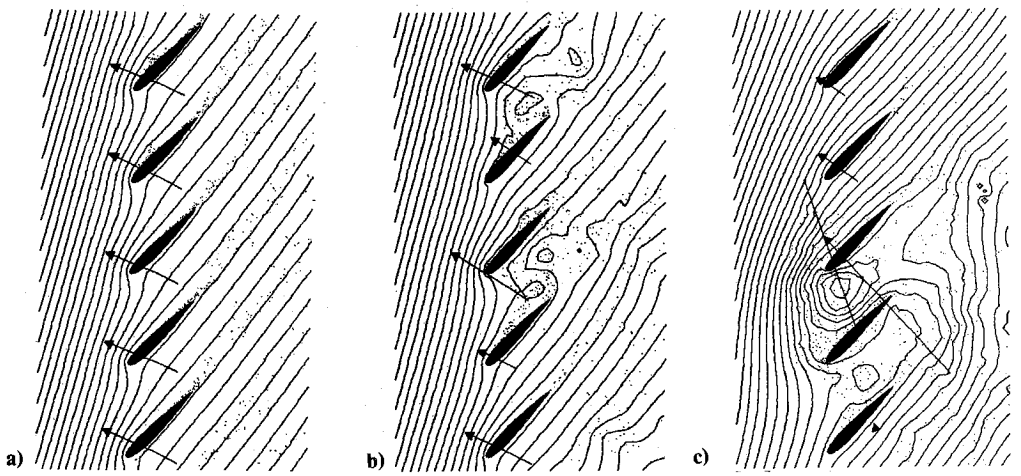

Fig. 14 Simulation with increasing angle of attack: a) $t=23.94$, b) $t=37.90$, c) $t=53.90$.

The importance of the initial disturbance, or seed, was investigated with $\beta=45$ deg, $\alpha=30$ deg (this experiment was suggested by a reviewer). When the seed is not included, the nonuniform flow pattern still develops, just more slowly. Shortly after the impulsive start, the flow is separated over all the blades and the circulation is established rapidly (Fig. 13a). However, the flow becomes noticeably different from blade to blade in a matter of a few time units: this is probably due to the merging of the vortices. The mergings depend on the ordering of the vortices, which is roughly from the bottom to the top of the figure. Thus a weak numerical disturbance has replaced the dipole or seed as the source of nonuniformity. Removing this numerical disturbance would require fairly major modifications to the code. After about 10 time units the flow exhibits two stall cells of uneven size (Fig. 13b). The weaker cell then disappears, and the one-cell pattern is fully established after about 20 time units (Fig. 13c). The flow seems to lose memory of its initial condition rather rapidly.

In view of this result, one is entitled to ask whether the instability of the blade-to-blade periodic flow is physically meaningful or just a numerical artifact. Three partial answers can be given to this question. First, numerical instabilities usually result in a solution that grows out of bounds. This is not the case here: a wave of finite amplitude is observed, and this amplitude saturates and remains roughly constant over many time units (the simulation has been extended beyond 150 time units in some cases). Second, the instability occurs or does not occur depending on small changes in the geometry, like a 5 deg change in angle. All the simulations used the same time step, vortex core size, distribution of points along the airfoil, etc. In other words, the numerical parameters were exactly the same. Finally, the comparison with experimental results, although limited, is satisfactory.

The inception of rotating stall was also studied with a time-varying angle of attack; this simulates the situation in a compressor when the throttle is being closed (this experiment was suggested by another reviewer). β was 45 deg and α rose from 25 deg to 30 deg, so that the flow crossed the stall boundary. The initial condition was the fully established, attached flow at $\alpha=25$ deg (compare Fig. 6a). As the angle of attack rose, two of the blades started stalling (Fig. 14a), and again two stall cells were observed (Fig. 14b). Finally, one of the cells dominated, and the eventual flow pattern was the same as before (Fig. 14c). This one-cell pattern has thus been reached through three different paths. It is possible that the 2-cell/5-blade pattern is linearly more unstable, but that the 1-cell/5-blade pattern dominates when the amplitude of the disturbance is large.

IV. Conclusions and Recommendations

The application of the vortex method to the flow in cascades has been presented. Rotating stall is observed, in staggered cascades, and the flow pattern agrees well with the experimental pattern. Rotating stall can occur in the absence of compressibility, rotation, three-dimensionality, and upstream disturbances. It seems to be a rather general phenomenon: within the range of angles that was explored, the stall pattern is always uneven, and always travels along the cascade.

Quantitative comparison with experiments was not attempted. The time-average results associate rotating stall with a decrease in the pressure rise across the cascade, and a dramatic

increase in the loss of total pressure. The stall boundary is sharp and indicates that stall is strongly influenced by the angle of attack and weakly influenced by the stagger.

Most of the simulations used five independent blades per period and eventually exhibited only one stall cell, but rotating stall is possible with as few as three blades per period. The inception of rotating stall was simulated under various conditions, and in several cases the flow first developed two cells which subsequently merged into one. Rotating stall does not seem to require a very specific wavelength.

In addition to the study of the inception mechanism, future work using the present method could explore the effects of the airfoil, of the solidity, and of the computational period. The rotating stall pattern might have a preferred wavelength, or it might always expand to the size of the period. The computer program used for this study is available for researchers interested in pursuing these investigations.

References

[1]Spalart, P. R. and Leonard, A., "Computation of Separated Flows by a Vortex Tracing Algorithm," AIAA Paper 81-1246, 1981.

[2]McCroskey, W. J., Spalart, P. R., Laib, G. H., Maisel, M. D., and Maskew, B., "Airloads on Bluff Bodies, with Application to the Rotor-Induced Downloads on Tilt-Rotor Aircraft," *Proceedings of the 9th European Rotorcraft Forum* and NASA T. M. 84-401, 1983.

[3]Chorin, A. J., "Numerical Study of Slightly Viscous Flow," Part 4, *Journal of Fluid Mechanics*, Vol. 57, 1973, pp. 785-796.

[4]Spalart, P. R., Leonard, A., and Baganoff, D., "Numerical Simulation of Separated Flows," NASA T. M. 84328, 1983.

[5]Lamb, H, *Hydrodynamics*, 6th ed., Dover Publications, New York, 1945, p. 224.